Metallurgical and Materials Engineering *Research paper*
Association of Metallurgical Engineers of Serbia AMES *https://doi.org/10.30544/640*

CORROSION AND WEAR PERFORMANCES ANALYSIS OF PVD CrMoN/Cr COATINGS

Kheireddine Bouzid[1,2], Rim Lamari[3], Nasser Eddine Beliardouh[2], Corinne Nouveau[4], Barnali Biswas[5]*

[1]Department of metallurgy, BADJI Mokhtar University of Annaba, BP12, 23000 Algeria
[2]Laboratoired'Ingénierie des Surfaces (LIS), BADJI MokhtarUniversity of Annaba, BP12, 23000 Algeria
[3]Laboratory of environmental engineering, BADJI MokhtarUniversity of Annaba, BP12, 23000 Algeria
[4]Arts et Metiers Institute of Technology LaBoMaP, Rue Porte de Paris 71250 Cluny, France
[5]Department of Physics, University of Calcutta, Diamond Harbour, South 24 Parganas, 743331, West Bengal, India

Received 28.04.2021
Accepted 08.08.2021

Abstract

Tools coated CrN based alloys are currently used in several industries for machining and manufacturing but present severe wear, limiting their service life. Seeking an alternative, three CrMoN monolayers (~1- 1.8 µm in thickness) coatings varying in the Mo percentage content were elaborated using the RF magnetron co-sputtering method. These coatings were evaluated and compared with the alloy currently used (CrN) by electrochemical tests in NaCl solution (stationary and no stationary methods) and sliding wear tests (ball-on-disc configuration) performed at room temperature. The results indicate that the samples coated with CrMoN presented better performance against wear and corrosion than the uncoated sample. Among the coatings, labeled C1 (27Mo at.%) showed the best corrosion resistance as it presents a positive corrosion potential E_{corr}. However, the best wear resistance (lowest coefficient of friction) was shown by coating labeled C4 (33Mo at.%). All of the tested specimens underwent abrasive wear in addition to the adhesive wear.

Keywords: PVD coating; CrMoN; wear; corrosion.

*Corresponding author: Kheireddine Bouzid, *kheiro.bouzid@yahoo.fr*

Introduction

Nowadays, surfaces are of great importance in the conception and design of new materials. In this modern world, materials face new situations every day, and the surface of the material represents the pathway through which material interacts with the environment. Thus, it is especially important to obtain a material with high surface quality to ensure befitting properties and functions as required.

Different techniques of surface treatments are evolved to improve specific surface properties. Surface coating is one of these strategies, which proved its efficiency and effectiveness. Among several techniques for surface coating, physical vapor deposition (PVD) is one of the principal methods used to coat a wide range of materials. Moreover, these PVD coatings are well suited for various applications in a wide variety of environments. The development of wear reducing coatings has started with tool coating [1]. Today, there exist broad varieties of tool coatings for nearly every demand.

In tools for machining, manufacturing and tools for forming complex parts for many applications as well as in mechanical engineering fields, the PVD methods are one of the technologies that improve tool life and productivity [2]. *L. Fedrizzi et al.* [3] reported that 80% of the total cost for protecting metals is related to coating application.

TiN and CrN based coatings, elaborated by PVD methods, are recognized as the most effective prevention against wear and corrosion in the tool manufacturing area. Besides, they display high mechanical properties (hardness, elastic modulus, toughness) as well as thermal stability [4]. To further upgrade, the mechanical and the electrochemical properties, two principal ways have been (in general) proposed in the literature [5]. The first one is based on adding another element (or more) into the CrN (TiN) coating; numerous combinations such as CrAlN, CrVN, CrMoN, CrZrN [6] are actually in the market. The second way was depositing two kinds of nitride coatings alternately, such as CrN/AlN systems [7] in the form of the multilayer or superlattice arrangements. It was reported in the literature that both the process parameters and thickness of the PVD coating had a direct influence on the microstructure and the residual stress state. Usually, the thicker the coating, the larger the residual tensile stress accumulation and the worse the adhesion to the substrate [8]. Optimizing the coating parameters permits a reduction in the number of defects through the control of the structure and the stoichiometric composition [9].

In the particular case of the Mo addition in CrN based coatings, it was observed an increase in the wear performances of machining tools. The Mo atoms offer more crystallinity, and better homogeneity of physical vapor deposited CrN coatings due to the formation of solid solution phases, including Mo_2N, CrMoNx, and Cr_2N [10].

CrMoN are among the common commercial coatings available for tribological applications because they require minimal to no post-deposition processing. The properties of coatings, including their tribological properties, will be influenced by the microstructure. It was reported that the self-lubricating MoO_3 phase could forms during the tribological process [11], thus diminishing the friction force and reducing the coefficient of friction. *Cheng Luet al.* show that the CrMoN coating (18.20 at.% Mo) exhibited the best tribological behavior property at 700 °C [12]. Regarding the mechanical properties, the addition of the Mo element improves the hardness (H = 34 GPa) of the CrMoN coating (21 at.% Mo) while only H = 18 GPa was obtained for pure CrN. Besides, it reduced the corresponding friction coefficient from 0.49 (pure CrN) to 0.37 (CrN with incorporating 30.4 at.% Mo) [13].

The corrosion performance of the CrMoN coatings is found to be superior to CrN coatings (free of Mo). This is because CrMoN coatings are much denser, more compact, i.e., these coatings have fewer pores, droplets, and other coating defects [14]. *Jie et al.* showed the best corrosion resistance in CrMoN coating with 16.20 at.% Mo, when compared to 7.20 Mo at.% and 20.20 Mo at.% [15].

This work was done based on the reviewed literature and in the focus to obtain an acceptable Quality/Price ratio of manufacturing industrial machining tools. Through previous analysis, it was found that the prepared CrMoN coatings had good mechanical properties; hardness (H), elastic modulus (E), and adhesion strength [16]. That is why the objective of this study is to improve CrMoN monolayer-coated tool performances. The influence of the Mo content on the resistance against corrosion and wear of PVD CrN coatings in severe conditions was analyzed and compared to a reference CrN (0% Mo) coating.

Experimental procedures

Coating deposition

Nanostructured Cr/CrMoN coating was deposited using RF dual magnetron sputtering system (NORDIKO 3500–13.56 MHz, 1250 W). Pure Cr (99.9%) and Mo (99.95%) targets (101.6 mm in diameter, 3 mm thickness) were used to deposit these coatings. During deposition, high purity argon and nitrogen (99.99%) were introduced into the chamber. To obtain desired chemical compositions, Mo target bias was adapted from 0 V to -900 V.

Two types of substrates were used in this study. The first one is a commercial tool steel (90CrMoV8) destined to tribological tests, with the following approximate chemical composition as provided by the manufacturer (in wt.%): (C = 0.5; Mn = 0.5; Si = 1; Cr = 8; Mo = 1.5; V = 0.5, and Fe = Balance). The second substrate was an amorphous glass type intended for electrochemical tests. During deposition, the targets/substrates distance was fixed at 90 mm.

Chromium and Molybdenum targets were co-sputtered at an optimized sputtering rate to yield thick films less than 2 µm of desired CrMoN coating. Such a ternary system is compositionally close to the 90CrMoV8 steel substrate and may have the potential for improving the tribological performance of tools when compared to binary CrN or MoN coating systems. The choice of selected parameters is based on previous works [16]. With the increase in the Mo bias voltage, the chemical composition of the CrMoN varied between Mo=19 at.% and 33 at.%. In parallel, a variation of the N content is observed, and it varies between 31 to 39 at.%. The chemical compositions of different samples obtained by EDS analysis (O_2 % =balance), are depicted in Table 1

Before the deposition, the vacuum chamber was pumped down to $2 \cdot 10^{-4}$ Pa. The substrates and the targets were then in situ etched for 5 min using argon ions.

The working pressure, the N_2 content in the plasma, and the deposition time were constant and equal to 0.4 Pa, 20%, and 90 min, respectively. The deposition time includes 10 min of Cr metallic layer (adhesion layer) and 80 min of deposition with a reactive nitrogen atmosphere.

Corrosion tests

The corrosion test is one of the most important criteria to evaluate the performance of the material tools in an aqueous solution, especially in the presence of Cl^- aggressive ions.

The corrosion study was carried out with a *Gamry unit, model PCI 4*, utilized for DC and AC measurements. Electrochemical Impedance Spectroscopy (EIS) and Tafel polarization curves were obtained at room temperature, using a three-electrode system. It consists of the elaborated specimen as a working electrode, saturated calomel electrode as a reference electrode, and a platinum wire as a counter-electrode. The exposed area to the corrosive medium was approximately 0.5 cm^2. All the electrochemical tests were performed in a 3.5% NaCl solution under free air condition at room temperature (22-25 °C) and 40-50 relative humidity. To establish the open-circuit potential (OCP), the sample was immersed for 60 min in the solution before corrosion tests. Electrochemical Impedance Spectroscopy was performed at a frequency sweep ranging from 100 kHz to 0.01 Hz with a data density of 5 points per decade. The applied alternating potential had an amplitude of 30 mV applied to the working electrode and reference electrode. After the open circuit voltage values were established, the EIS measurements were initiated. To obtain the Tafel polarization method was carried out under a voltage sweep at a speed of 15 mV/mn in the range of ± 0.4V *(vs*. OCP). The corrosion potential (E_{corr}) and the corrosion current density (i_{corr}) were deduced from the Tafel plot. The corrosion current is obtained using the Stern–Geary equation [17]

$$Icorr = \frac{\beta a.\ \beta c}{2{,}303\ (\beta a+\beta c)} \frac{1}{Rp} \qquad 1$$

-βa and βc are the Tafel slopes, a and c subscript are "anodic" and "cathodic" branches expressed in V/decade (V/dec)

-Rp is the polarization resistance expressed in Ω.cm^2, calculated using the following equation:

$$Rp = \frac{\Delta E}{\Delta I} \qquad 2$$

Where ΔE is the polarization potential, and Δi is the polarization current.

Tribological tests

The tribological properties of the coatings are evaluated under dry sliding conditions at room temperature using a CSM ball-on-disc tribometer (*CSM HT 1100*) and *Tribox 4.1.1* software. Samples are tested against an Al_2O_3 ball with 6 mm diameter, arithmetic surface roughness *R*a= 388.57 nm, and hardness (H) of 13 GPa. The applied load was 2 N at a constant sliding speed of 2 cm/s and a total sliding distance of 50 m.

Results and discussion

Microstructural analysis

In addition to the chemical compositions, table 1 also shows thickness, and growth rate of the synthesized specimens. The morphology and the thickness of the obtained layers were analyzed by SEM (JEOL *JSM-5900-LV* microscope) equipped with an energy dispersive spectroscopy (EDS). The electron energy was 5 keV, and the standard deviation of composition quantification was less than 1 at.%. As can be seen, coating thickness changes with the concentration of Mo, and the thickness values are found to be in the range from 0.8 µm (Mo = 33%) to 1.8 µm (Mo = 0%). The growth rate parameter and the coating thickness decrease as the Cr content decreases.

Table .1 Coating characteristics

Coatings	Bias Voltage (V)		Chemical composition (at.%)			Thickness (µm)	Growth rate (µm/min)
	Cr	Mo	Cr	Mo	N		
C1	-900	0	64	0	30	1.89	0.021
C2	//	-500	42	19	31	1.33	0.014
C3	//	-700	35	27	32	1.07	0.011
C4	-700	-900	19	33	39	0.787	0.008

Microstructural analysis displays no visible difference among the obtained microstructures.

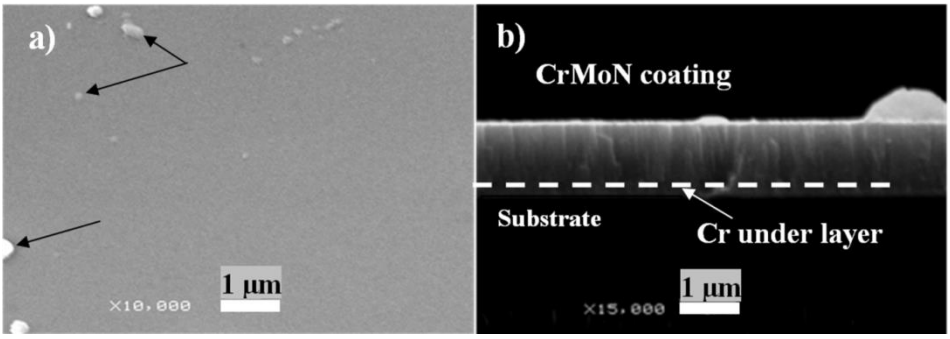

Fig. 1. SEM micrographs of the CrMoN-C2 coating; (a) superficial aspect and (b) the cross-section view.

All specimens showed similar superficial aspects and structure growth. Figure 1 shows SEM micrographs of the C2 specimen, taken as an example. The superficial aspect of the coating (Figure 1a) shows a dense microstructure with a dome-shaped morphology. It illustrates the successful fabrication of a quasi-pore-free coating. Of course, some inevitable defects (droplets) are apparent, as indicated by arrows in Figure 1. The cross-sectional micrograph (Figure 1b) shows good adhesion of the coating to the substrate. Figure1b also presents the monolayer film with a columnar microstructure growth of the (CrMoN) film (thickness of 1.33 ± 0.05 µm), including the metallic layer adhesion of Cr around 0.2 ± 0.02 µm in thickness.

Electrochemical performances

Figure 2 shows the Tafel plots obtained for all of the tested specimens. Generally, the cathodic region of the polarization curve describes the cathodic hydrogen evolution reaction associated with water reduction and the anodic part of the polarization curve represents the dissolution of the sample at an elevated potential.

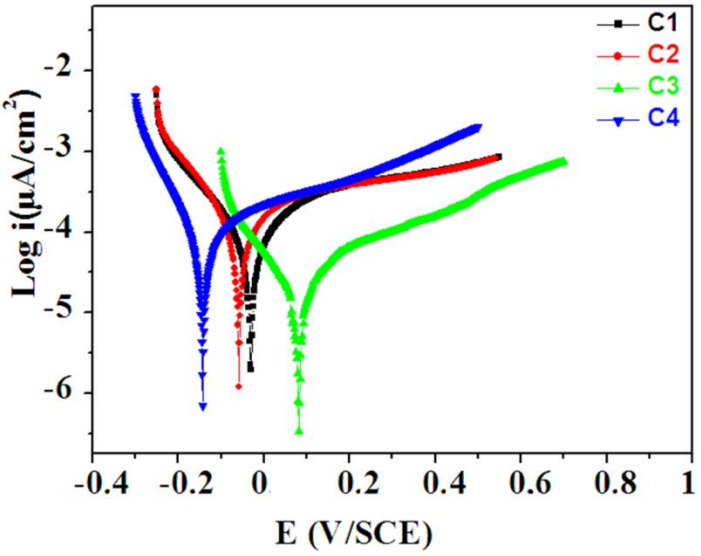

Fig. 2. Potentiodynamic polarization curves corresponding to the different coatings tested in 3.5% NaCl. Sample C1 (CrN 0% Mo) is included as a reference.

In comparison, the cathodic branch of C3 shifts towards a lower current density than both of C2 and C4 specimens as well as the CrN reference sample, indicating that the cathodic hydrogen evolution reaction is suppressed on C2. All the curves showed a plateau indicating high corrosion resistance due to a passive film formation over the surface. It is visible that the curve of C3 coating manifests a more positive corrosion potential and a higher corrosion resistance.

Table 2 summarizes the results of the potentiodynamic tests based on the Tafel extrapolation method. It can be seen that the C3 specimen has positive E_{corr}(~ +26 mV/ECS) and the lowest i_{corr} (0.45 μA/cm^2) as expected. The CrN coating (taken as reference) indicates the lesser corrosion resistance (highest i_{corr} value) compared to other coatings. Therefore, one can note that the Mo content has a beneficial effect on the corrosion resistance of the CrN based coatings. It is well known that high corrosion current density translates to the higher anode dissolving of the coating and leads to poor corrosion protection properties. Inversely, low current density gives high resistance to polarization (Rp); The Rp value of C3 is higher than the reference (CrN specimen) by factor six. Therefore, these results are in good agreement with numerous works [18].

Table. 2. Potentiodynamic polarization data of the tested specimens.

Coatings	i_{corr} ($\mu A/cm^2$)	E_{corr} (V)	Rp ($K\Omega \cdot cm^2$)
C1	4,13	-0. 051	11,797
C2	3,28	-0. 084	13,730
C3	0,45	+0. 026	76,065
C4	0,60	-0. 17	49,559

Figure 3 displays an example of the surface appearance of sample references C1 (the poorest corrosion resistance) and C2 coating (the best corrosion resistance) after polarization tests. As demonstrates circled zones (Figure 3a-b), surfaces are composed of intact regions (free of pits) and corroded regions "concentration of holes and pits". So, it can be concluded from the above observation that after polarization tests, all of the specimens showed evidence of localized corrosion i.e., pitting corrosion.

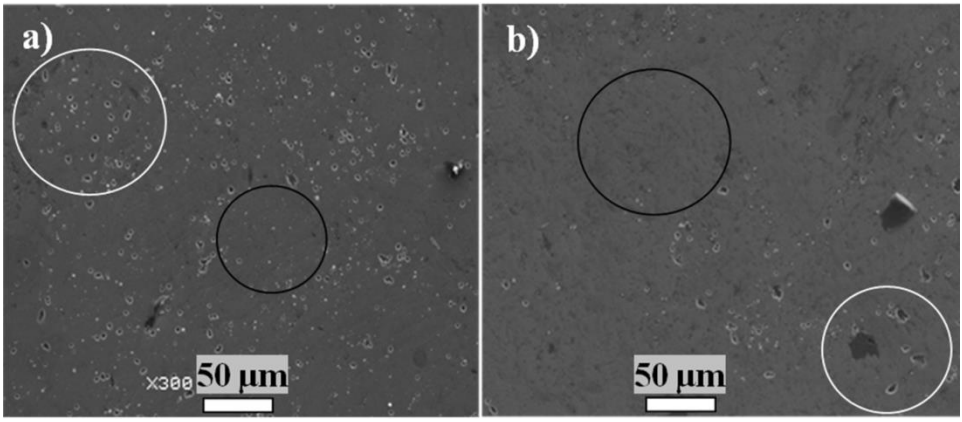

Fig. 3.SEM micrographs of the coating specimens C1 (a) and C2 (b) after polarization tests in a 3.5% NaCl solution. Example of a corroded region (white circle) and an intact region (black circle).

The EIS measurement is considered a non-destructive technique. It represents the most adequate technique to clarify the corrosion mechanism in the electrolyte/coating interface [19]. Figure 4 shows the Nyquist and the Bode plots of the tested coatings acquired in 3.5% NaCl solution after 2 h of immersion at open circuit potential. The Nyquist plots (Figure 4a) are in the form of "arcs". Only a single "arc" for each sample was depicted.

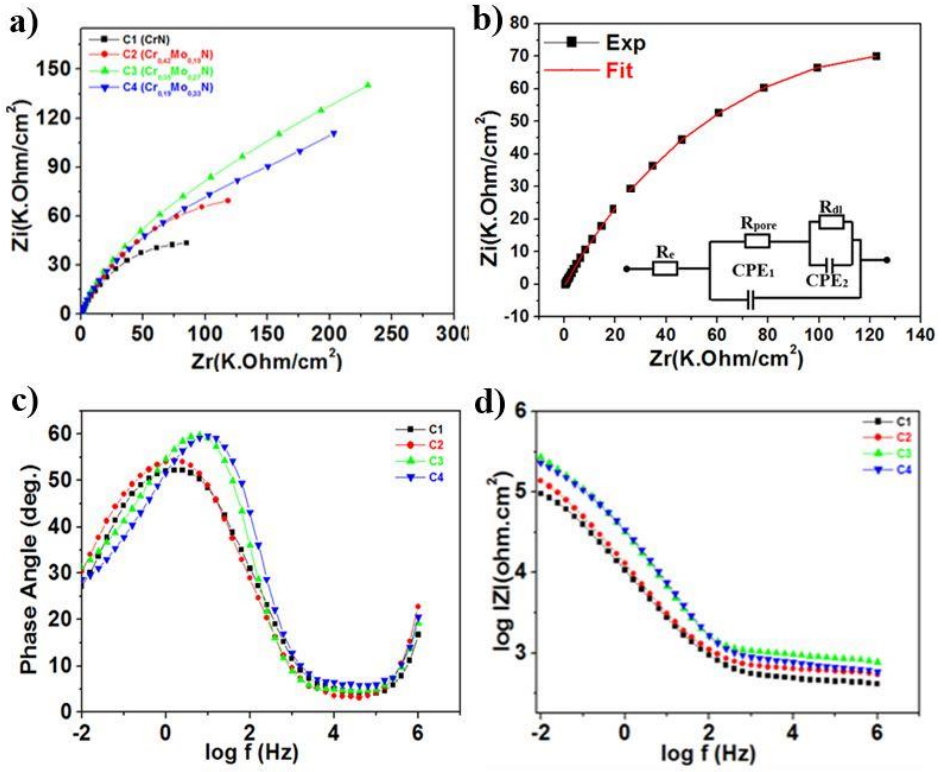

Fig. 4. EIS spectra (a) Nyquist plots (b) example of C2 fitted curve: Nyquist experimental (black) and modeling curves (in red) and the EEC model (c, d) Bode plots of the tested coatings in 3.5% NaCl solution.

However, the radii of the arcs are different, which suggests different corrosion rates of the tested coatings. The capacitive arc, in the higher frequency region, is associated with the charge transfer resistance. This is because of the resistance during electron transfer in the Faradic process in parallel to the double-layer capacitance at the interface between the surface of the coating and the saline solution. The larger radius of the capacitive arc indicates the greater resistance to the electrochemical reaction on the electrode surface [20]. Obviously, the Nyquist curves of the C3 and C4 samples represented the highest impedance level and advanced corrosion resistance. However, when considering the Bode plots (Figure4 c-d), a second loop appears at low frequencies. That is why it is recommended to consider both the Nyquist and Bode representations.

To evaluate the quantitative EIS response, diagrams were fitted using *ZView Software* based on an electrical equivalent circuit (EEC) as depicted in Figure 4b. The proposed EEC was chosen based on reviewed literature [17, 21-26]. Besides**,** fitting results showed in Figure 4b, ascertained the goodness and congruence between experimental and fitted data. The EES shown in Figure 4b represents the electrolytes, while R_{pore} and R_{ct} are the micro-pore and charge transfer resistance, respectively. CPE1

and CPE2 are the interface solution-multilayer and the double-layer capacitances, respectively.

CPE1-R1 couple predominates at high frequencies, is possibly originated by the passive coating, while the CPE2-R2 couple, controlling at low frequencies, characterizes the corrosion process of the substrate/film pore solution interfaces, as reported by [27-28].

R_{ct} is the major parameter for corrosion evaluation. The larger R_{ct} related, the better corrosion resistance [15]. Therefore, the C3 coating has the largest Rct (1.9 106Ω.cm2). This is in good agreement with potentiodynamic results (i_{corr} tendency in Table 2).

Table 3 summarizes the quantitative analysis of EIS results by fitting the EEC on the EIS data. Depending on the surface roughness, the 'n' value changes from 0 to 1 [29]. For a perfect surface, when the value of n=1, the impedance of CPE is that of a pure capacitor. When n = 0.5, it indicates a diffusion-controlled process or a porous material.

Table 3. Optimized values for the equivalent circuit parameters obtained by ZView program.

Coatings	Rs ($K\Omega\cdot cm^2$)	CPE1		R_{pore} ($K\Omega\cdot cm^2$)	CPE2		R_{ct}($K\Omega.cm^2$) , 10^3
		C_{coat} ($\mu F/cm^2$)	n_1		C_{dl} ($\mu F/cm^2$)	n_2	
C1	0.43	21.60	0.61	5. 63	6.959	0.774	0.14
C2	0.42	19.84	0.64	7.65	4.107	0.48	0.33
C3	0.46	5.48	0.79	30. 66	8.291	0.351	1.89
C4	0.44	5.51	0.77	57. 69	11.21	0.348	1.67

When 0.5 < n < 1, the deviation from the ideal behavior is ascribed to a heterogeneous rough electrode, a non-homogeneous current distribution on the electrode surface, a non-homogeneous distribution of the electrical properties within the oxide film or within the coating [30–31]. EIS measurements are in agreement with data obtained by potentiodynamic analysis. C3 specimen presents the higher corrosion resistance among tested specimens. Introducing Mo (27 at.%) improved corrosion resistance of CrMoN coating in aggressive Cl^- medium.

Tribological performances

Figure 5 shows the friction coefficient evolution measured by pin-on-disc tests in dry sliding conditions. At the steady-state, one can see that the average value of COF decreases as the Mo content increases. The highest value of the mean-steady COF (0.68) is shown by the C2 specimen (0.19% Mo), while the lowest (0.45) is shown by C4 (0.33% Mo). The CrN coating reference remains integrity because its friction coefficient keeps stable (0.51) during the whole friction test. All the tested specimens present the same curve tendency (all plots are similar in shape) characterized by a short running followed by an abrupt increase at the final state.

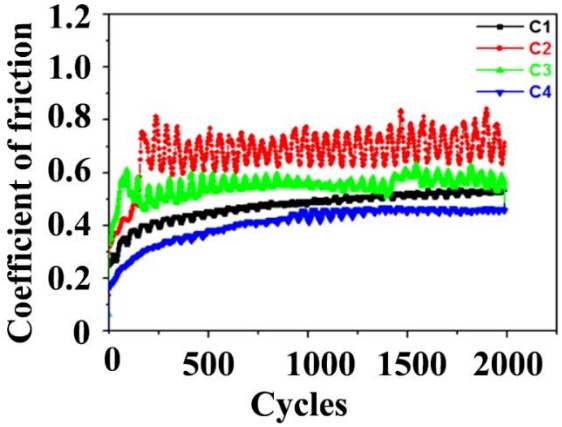

Fig. 5. Coefficient of friction vs. sliding distance (cycles)evolution of different samples against alumina ball in dry conditions.

Figure 6 indicates the wear tracks of the C2 (Figure 6a, b) and the C4 (Figure 6d, e) specimens. The same features are seen on the C1 and C3 specimens. Parallel grooves in the sliding direction can be clearly observed on the worn surfaces of all tested samples. It is the sign of abrasive wear (Figure 6a, b, d, e).

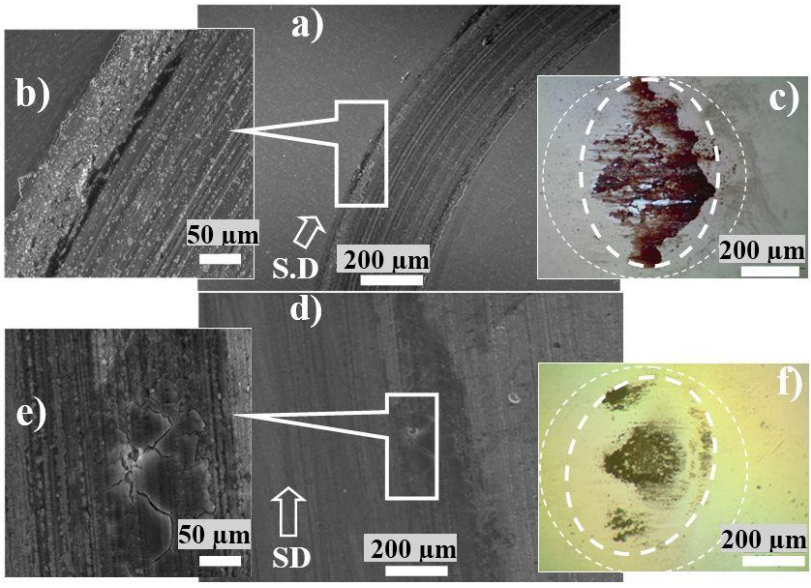

Fig. 6.SEM images of wear track against Alumina ball; (a-b) C2 and (d, e) C4. (c, f) optical images of the wear scar of the alumina ball after tribotests against C4 and C2 samples, respectively.

High magnified images (Figure 6b, e) reveal the plastic deformation and delamination of the film at the edges of the wear tracks. Moreover, the accumulation of

debris and the number of trapped particles inside grooves can also be noticed from these images.

Figure 6d presents cracks and "ships" formation. This is the proof of oxide film formation during the sliding test. It is the consequence of an increase in temperature when coating rubs against an alumina ball. After more and more sliding cycles, oxide film becomes brittle (cracks) and transforms into debris.

Optical microscopy analysis of the counter faces reveals that the wear scars of the counter-parts (Fig 6c, f) were covered by adhered material (from the coating specimens). This indicates that the adhesion wear mechanism happened under the present test condition for all tested samples. After cleaning, microgrooves were also detected on the wear scars of alumina balls. Third-body abrasive wear occurred when the coatings (C2 and C4) were sliding against the alumina balls; in addition, there is evidence of adhesive wear. The same mechanism occurs with C1 (C3)/alumina ball couples. Therefore, it can be claimed that the addition of Mo improves the tribological performance of CrN coating. The COF decreases as the Mo content increases. The principal wear mechanisms are abrasion and adhesion.

Discussion

From the above, the CrMoN coating shows a considerably improved performance with respect to the binary CrN. CrMoN samples presented corrosion current density up to four times lower than those obtained for the base CrN. Besides, the corrosion potential E_{corr} has reached a positive value in the C3 case. The excellent resistance against corrosion in the conditions selected in this study from the CrMoN has to be attributed to the microstructure (much denser and finer than CrN), thus to the chemical composition, i.e., the Mo content, because denser microstructure restricts the oxygen diffusion to the coating/substrate interface. These results are similar to those reported by *J. Jin et al.* in acidic media [ref]. The increase in corrosion performances was attributed to the incorporation of Mo, which makes the surface of Mo-doped CrN coating is denser and more homogeneous than CrN coating [14].

On another side, nowadays, it is well known that the corrosion resistance afforded by multilayer coating is better than single-layer coating because the great number of interfaces acts as a barrier, and it prevented the electrolyte from reaching the substrate via defects such as pores and droplets. The literature agrees that the electrochemical behavior is mainly controlled by passive film formation upon the outer layer [9]. Thus, the present study shows the possibility of obtaining single-layered coating with small thickness but similar protective properties to those hitherto described for multilayer coating. Therefore, this may be seen as an economic advantage.

As regards the mechanical properties and wear characteristics, comparable studies of multi-layered CrN/MoN and composite structures of Cr–Mo–N formed by sputtering or a hybrid PVD method have been reported [32]. *S.J. Heo et al.* reported the bias voltage effects on the friction behavior on the ternary Cr-Mo-N system [ref]. The COF tendency decreases from ~ 0.65 (-100V) to ~0.5 (-300V) while the film specimens formed at -400V bias conditions show higher friction coefficients ~0.7 [33]. Results obtained in this study indicated an increase in COF as the bias voltage increases (C2=0.68 at -500V and C3=0.5 at -700V) greater than the CrN coating reference. The specimen fabricated under -900V of bias conditions displays the lower friction coefficients (~0.45 33Mo). This phenomenon was also encountered by *C. Lu et al.* [12]

when investigating friction performances of CrMoN/MoS2 composite coatings. Despite MoS2 (lubricant), obtained results at room temperature are close to those reported here. The COF reached a maximum value (~ 0.67) at Mo= 29.7 at.% and decreased to ~0.44 for a sample with Mo = 37 at.% [12].

In agreement with [33], the different friction coefficients evolution between the film specimens, with different Mo content, can be explained by the different microstructural evolution of each film specimen. In particular, droplets could act as significant obstacles to increase friction on the film surface.

Conclusion

The properties of CrMoN films, depositing by RF reactive magnetron sputtering on tool steel and silicon substrates with different deposition parameters (Mo bias voltage) at room temperature, have been investigated. The microstructural results showed dense columnar microstructures. The potentiodynamic polarization measurement in 3.5% NaCl solution indicates that Mo addition to CrN can significantly improve the corrosion resistance. Among the samples, C3 specimen shows the optimal corrosion resistance among the samples with a positive E_{corr}(~ +26 mV/ECS) and the lowest i_{corr} (0.45 µA/cm^2). The dry sliding wear resistance tests indicated that the average value of COF decreases as the Mo content increases. Consequently, sample C4 specimen (Mo=33 at.%) exhibits the best anti wear properties. It has the lowest COF (~0.45).The principal wear mechanisms evolved during sliding against alumina balls are abrasion and adhesion.

Acknowledgments

The authors would like to thank the Algeria Ministry of Higher Education and Scientific Research MESRS and DGRSDT for supporting this work (PNE program 2019-2020). The authors are also grateful to colleagues from LaBoMaP (Arts & Métiers -Institute of Technology, Cluny, FRANCE) and Prof. S. ABDERRAHMANE from LIS laboratory Annaba, ALGERIA) for providing facilities to carry out this work.

References

[1] K. Bobzin, E. Lugscheider, R. Nickel, N. Bagcivan, A. Kramer: Wear, 263 (2007) 1274–1280.
[2] V. Prabakaran: J Bio TriboCorros, 4 (2018) 65.
[3] L. Fedrizzi, S. Rossi, R. Cristel, PL. Bonora: ElectrochimActa, 49 (2004) 2803–2814.
[4] L.Wang, D.O. Northwood, X. Nie, J. Houden, E. Spain, A. Leyland, et al.: J. Power Sources, 195 (2010) 3814–3821.
[5] G. Cabrera, F. Torres, J.C. Caicedo, W. Aperador, C. Amaya, P. Prieto:J. Mater. Eng. Perform, 21 (2012)128–136.
[6] Z. Kangpei, L. Ping, L. Wei, M. Fengcang, L. Xinkuan, C. Xiaohong: Appl. Surf. Sci, 257 (2011) 9583-9586.
[7] J. Lin, J.J. Moore, B. Mishra, M. Pinkas, X. Zhang, and W.D. Sproul: Thin Solid Films, 517 (2009) 5798.
[8] C. Lorenzo-Martin, O. Ajayi, A. Erdemir, G.R. Fenske, R.Wei: Wear, 302 (2013) 963–971.

[9] A. Conde, C. Navas, A.B. Cristóbal, J. Housden, J. de Damborenea: Surf Coat Technol, 201 (2006) 2690–2695.
[10] K. Ibrahim, MM. Rahman, H. Taha, E. Mohammadpour, Z. Zhou, CY. Yin, et al.: Appl. Surf. Sci, 440 (2018) 1001-1010.
[11] Q. Dongli, L. Hao, W. Tiegang, P. Zhiliang, G. Jun, S. Chao:J Mater Sci Technol, 31 (2015) 55-64.
[12] C. Lu, J. Jia, Y. Fu, G. Yi, X. Feng, J. Yanget al: Surf Coat Technol, 378 (2019) 125072.
[13] K.H. Kim, EY. Choi, SG. Hong, BG. Park, JH. Yoon, JH. Yong: Surf Coat Technol, 201 (2006) 4068–4072.
[14] J. Jin, H. Liu, D. Zheng, Z. Zhu: Int. J. Hydrog. Energy, 43 (2018) 10048-10060.
[15] J. Jin, X. Zhao, H. Liu: Int. J.Hydrog. Energy, 44 (2019) 20293-20303.
[16] Y. Zou, M.J. Walock, S.A. Catledge, C. Nouveau, A. Stanishevsky: J. Achiev. Mater ManufEng, 37 (2) (2009) 369 –374.
[17] G.V.K. William, C. Harish, S.V. Ezhil, S. Kalavati, K.S. Rajam: Thin Solid Films, 514 (2006) 204-211.
[18] Y.H. Yoo, J.H. Hong, J.G. Kim, H.Y. Lee, J.G. Han: Surf. Coat. Technol, 201 (2007)9518-9523
[19] M.S. Parviz, F.A. Arash, E. Hassan, I. Omid, N. Meisam: Surf. Interfaces, 21 (2020) 100721.
[20] T. Kattareeya, V. Patama, Y. Niti, L. Gobboon: Surf. Coat.Technol, 358 (2018) 732-740.
[21] Y. Chengtong, J. Lina, X. Gaoxiang, W. Fangfang, W. Xinchao, Z. Hu: Surf Coat Technol, 366 (2019) 214-226.
[22] Q. Yanfang, Z. Hongjian, L. Chao, L. Jinbin, H. Jining: Surf Coat Technol, 398 (2020) 126086.
[23] H.P. Jae, K. Daichi, H. Takeshi, K. Yuki, I. Ryoichi, H.L. Myeong: Surf Coat Technol, 389 (2020) 125567.
[24] W. Lijun, W. Mengchao, C. Hui:Surf Coat Technol, 391 (2020) 125660.
[25] D. Jin, Z. Jianfeng, X. Jinyong, Z. Chao: Ceram.Int, 46 (2020) 21707-21718.
[26] F.C. Silva, O.M. Prada, M.A. Tunes, P.D. Edmondson, J.C. Sagas, L.C. Fontana, et al.: Int. J. Hydrog. Energy, 45 (2020) 33993-34010.
[27] W. Aperador, R. Mejía de Gutiérrez, D.M. Bastidas:Corros. Sci, 51 (2009) 2027-2033.
[28] J.M. Bastidas, M. Saiki, S.O. Rogero, I. Costa, J.L. Polo: J. Appl. Electrochem, 32 (2002) 487-496.
[29] S.D. Vishnu, S. Ramesh, T. Elangovan, A. Madhankumar, P. Kwideok, M. Zuhair: Appl. Surf. Sci, 371 (2016) 262–274.
[30] R.N. Peres, E.F. Cardoso, M. Montemor, H.G. De Melo, A.V. Benedetti, P.H. Suegama: Surf. Coat. Technol, 303 (2015) 372-384.
[31] A. Conde, J.J. De Damborenea: Corros. Sci, 44 (2002) 1555–1567.
[32] D. Yuelan, Z. Ping, C. Zhihai, Y. Zhen, L. Qi, S. Wei: Rare. Metal. Mat. Eng, 43 (2) (2014) 264–268.
[33] Su JH, Kim SW, Yeo IW, Park SJ, Oh YS: Int J Ceram, 42 (2016) 5231e7.